Research Article | Vol. 26, No. 13 | 25 Jun 2018 | OPTICS EXPRESS 16940

Optics EXPRESS

Tunable, omnidirectional, and nearly perfect resonant absorptions by a graphene-hBN-based hole array metamaterial

HODJAT HAJIAN,[1,*] AMIR GHOBADI,[1,2] BAYRAM BUTUN,[1] AND EKMEL OZBAY[1,2,3,4]

[1]*NANOTAM-Nanotechnology Research Center, Bilkent University, 06800 Ankara, Turkey*
[2]*Department of Electrical and Electronics Engineering, Bilkent University, 06800 Ankara, Turkey*
[3]*Department of Physics and UNAM-Institute of Materials Science and Nanotechnology, Bilkent University, 06800 Ankara, Turkey*
[4]*ozbay@bilkent.edu.tr*
**hodja.hajian@bilkent.edu.tr*

Abstract: In this paper, we propose an electrically tunable mid-infrared plasmonic-phononic absorber with omnidirectional and polarization insensitive nearly perfect resonant absorption characteristics. The absorber consists of a graphene/hexagonal boron nitride (hBN)/graphene multilayer on top of a gold bottom reflector separated by a dielectric spacer. The graphene/hBN/graphene multilayer is patterned as a hole array in square lattice. We analytically and numerically prove that, due to the support of hybrid plasmon-phonon-polaritons, nearly perfect multi-resonant absorption peaks with high quality factors are obtained both inside and outside of the Reststrahlen band of hBN. As a result of the hybridization of graphene plasmons with the hyperbolic phonon polaritons of hBN, the high quality resonant absorptions of the metamaterial are almost unaffected by decreasing the phenomenological electron relaxation time of graphene. Moreover, the obtained resonances can be effectively tuned in practice due to the continuity of the graphene layers in the hole array metamaterial. These features make the graphene-hBN metamaterial a skeptical design for practical purposes and mid-infrared multi-functional operations such as sensing.

OCIS codes: (160.3918) Metamaterials; (350.2450) Filters, absorption; (240.6680) Surface plasmons; (240.5420) Polaritons.

References and links

1. A. Boardman, "Pioneers in metamaterials: John Pendry and Victor Veselago," J. Opt. **13**(2), 020401 (2010).
2. P. Senanayake, C. H. Hung, J. Shapiro, A. Lin, B. Liang, B. S. Williams, and D. L. Huffaker, "Surface plasmon-enhanced nanopillar photodetectors," Nano Lett. **11**(12), 5279–5283 (2011).
3. J. R. Cole and N. J. Halas, "Optimized plasmonic nanoparticle distributions for solar spectrum harvesting," Appl. Phys. Lett. **89**(15), 153120 (2006).
4. A. Lochbaum, Y. Fedoryshyn, A. Dorodnyy, U. Koch, C. Hafner, and J. Leuthold, "On-chip narrowband thermal emitter for mid-IR optical gas sensing," ACS Photonics **4**(6), 1371–1380 (2017).
5. F. A. L. de Souza, R. G. Amorim, W. L. Scopel, and R. H. Scheicher, "Nano-structured interface of graphene and h-BN for sensing applications," Nanotechnology **27**(36), 365503 (2016).
6. K. Chen, R. Adato, and H. Altug, "Dual-band perfect absorber for multispectral plasmon-enhanced infrared spectroscopy," ACS Nano **6**(9), 7998–8006 (2012).
7. N. Mattiucci, M. J. Bloemer, N. Aközbek, and G. D'Aguanno, "Impedance matched thin metamaterials make metals absorbing," Sci. Rep. **3**(1), 3203 (2013).
8. H. Deng, Z. Li, L. Stan, D. Rosenmann, D. Czaplewski, J. Gao, and X. Yang, "Broadband perfect absorber based on one ultrathin layer of refractory metal," Opt. Lett. **40**(11), 2592–2595 (2015).
9. F. Ding, J. Dai, Y. Chen, J. Zhu, Y. Jin, and S. I. Bozhevolnyi, "Broadband near-infrared metamaterial absorbers utilizing highly lossy metals," Sci. Rep. **6**(1), 39445 (2016).
10. M. G. Nielsen, D. K. Gramotnev, A. Pors, O. Albrektsen, and S. I. Bozhevolnyi, "Continuous layer gap plasmon resonators," Opt. Express **19**(20), 19310–19322 (2011).
11. H. T. Chen, "Interference theory of metamaterial perfect absorbers," Opt. Express **20**(7), 7165–7172 (2012).
12. K. Aydin, V. E. Ferry, R. M. Briggs, and H. A. Atwater, "Broadband polarization-independent resonant light absorption using ultrathin plasmonic super absorbers," Nat. Commun. **2**(1), 517 (2011).

#328051 https://doi.org/10.1364/OE.26.016940
Journal © 2018 Received 10 Apr 2018; revised 4 Jun 2018; accepted 4 Jun 2018; published 18 Jun 2018

Optics EXPRESS

13. Y. Bai, L. Zhao, D. Ju, Y. Jiang, and L. Liu, "Wide-angle, polarization-independent and dual-band infrared perfect absorber based on L-shaped metamaterial," Opt. Express **23**(7), 8670–8680 (2015).
14. J. Kim, K. Han, and J. W. Hahn, "Selective dual-band metamaterial perfect absorber for infrared stealth technology," Sci. Rep. **7**(1), 6740 (2017).
15. X. Liu, T. Tyler, T. Starr, A. F. Starr, N. M. Jokerst, and W. J. Padilla, "Taming the blackbody with infrared metamaterials as selective thermal emitters," Phys. Rev. Lett. **107**(4), 045901 (2011).
16. C. Hu, L. Liu, Z. Zhao, X. Chen, and X. Luo, "Mixed plasmons coupling for expanding the bandwidth of near-perfect absorption at visible frequencies," Opt. Express **17**(19), 16745–16749 (2009).
17. M. G. Nielsen, A. Pors, O. Albrektsen, and S. I. Bozhevolnyi, "Efficient absorption of visible radiation by gap plasmon resonators," Opt. Express **20**(12), 13311–13319 (2012).
18. A. Ghobadi, H. Hajian, M. Gokbayrak, S. A. Dereshgi, A. Toprak, B. Butun, and E. Ozbay, "Visible light nearly perfect absorber: an optimum unit cell arrangement for near absolute polarization insensitivity," Opt. Express **25**(22), 27624–27634 (2017).
19. A. Ghobadi, H. Hajian, S. A. Dereshgi, B. Bozok, B. Butun, and E. Ozbay, "Disordered nanohole patterns in metal-insulator multilayer for ultra-broadband light absorption: Atomic layer deposition for lithography free highly repeatable large scale multilayer growth," Sci. Rep. **7**(1), 15079 (2017).
20. A. N. Grigorenko, M. Polini, and K. S. Novoselov, "Graphene plasmonics," Nat. Photonics **6**(11), 749–758 (2012).
21. T. Low and P. Avouris, "Graphene plasmonics for terahertz to mid-Infrared applications," ACS Nano **8**(2), 1086–1101 (2014).
22. H. Hajian, H. Caglayan, and E. Ozbay, "Long-range Tamm surface plasmons supported by graphene-dielectric metamaterials," J. Appl. Phys. **121**(3), 033101 (2017).
23. S. Thongrattanasiri, F. H. Koppens, and F. J. García de Abajo, "Complete optical absorption in periodically patterned graphene," Phys. Rev. Lett. **108**(4), 047401 (2012).
24. G. Yao, F. Ling, J. Yue, C. Luo, J. Ji, and J. Yao, "Dual-band tunable perfect metamaterial absorber in the THz range," Opt. Express **24**(2), 1518–1527 (2016).
25. A. Yu. Nikitin, F. Guinea, and L. Martin-Moreno, "Resonant plasmonic effects in periodic graphene antidot arrays," Appl. Phys. Lett. **101**(15), 151119 (2012).
26. P. Q. Liu, F. Valmorra, C. Maissen, and J. Faist, "Electrically tunable graphene anti-dot array terahertz plasmonic crystals exhibiting multi-band resonances," Optica **2**(2), 135–140 (2015).
27. R. Alaee, M. Farhat, C. Rockstuhl, and F. Lederer, "A perfect absorber made of a graphene micro-ribbon metamaterial," Opt. Express **20**(27), 28017–28024 (2012).
28. B. Deng, Q. Guo, C. Li, H. Wang, X. Ling, D. B. Farmer, S. J. Han, J. Kong, and F. Xia, "Coupling-enhanced broadband mid-infrared light absorption in graphene plasmonic nanostructures," ACS Nano **10**(12), 11172–11178 (2016).
29. H. Yan, T. Low, W. Zhu, Y. Wu, M. Freitag, X. Li, F. Guinea, P. Avouris, and F. Xia, "Damping pathways of mid-infrared plasmons in graphene nanostructures," Nat. Photonics **7**(5), 394–399 (2013).
30. H. Li, L. Wang, and X. Zhai, "Tunable graphene-based midinfrared plasmonic wide-angle narrowband perfect absorber," Sci. Rep. **6**(1), 36651 (2016).
31. X. Zou, G. Zheng, J. Cong, L. Xu, Y. Chen, and M. Lai, "Polarization-insensitive and wide-incident-angle optical absorber with periodically patterned graphene-dielectric arrays," Opt. Lett. **43**(1), 46–49 (2018).
32. X. Hu and J. Wang, "High-speed gate-tunable terahertz coherent perfect absorption using a split-ring graphene," Opt. Lett. **40**(23), 5538–5541 (2015).
33. X. Wang, X. Jiang, Q. You, J. Guo, X. Dai, and Y. Xiang, "Tunable and multichannel terahertz perfect absorber due to Tamm surface plasmons with graphene," Photon. Res. **5**(6), 536 (2018).
34. J. Guo, L. Wu, X. Daia, Y. Xiang, and D. Fan, "Absorption enhancement and total absorption in a graphene-waveguide hybrid structure," AIP Adv. **7**(2), 025101 (2017).
35. Y. Xiang, X. Dai, J. Guo, H. Zhang, S. Wen, and D. Tang, "Critical coupling with graphene-based hyperbolic metamaterials," Sci. Rep. **4**(1), 5483 (2014).
36. J. D. Caldwell, L. Lindsay, V. Giannini, I. Vurgaftman, T. L. Reinecke, S. A. Maier, and O. J. Glembocki, "Low-loss, infrared and terahertz nanophotonics using surface phonon polaritons," Nanophotonics **4**(1), 44–68 (2015).
37. J. D. Caldwell, A. V. Kretinin, Y. Chen, V. Giannini, M. M. Fogler, Y. Francescato, C. T. Ellis, J. G. Tischler, C. R. Woods, A. J. Giles, M. Hong, K. Watanabe, T. Taniguchi, S. A. Maier, and K. S. Novoselov, "Subdiffractional volume-confined polaritons in the natural hyperbolic material hexagonal boron nitride," Nat. Commun. **5**(1), 5221 (2014).
38. S. Dai, Z. Fei, Q. Ma, A. S. Rodin, M. Wagner, A. S. McLeod, M. K. Liu, W. Gannett, W. Regan, K. Watanabe, T. Taniguchi, M. Thiemens, G. Dominguez, A. H. Castro Neto, A. Zettl, F. Keilmann, P. Jarillo-Herrero, M. M. Fogler, and D. N. Basov, "Tunable phonon polaritons in atomically thin van der Waals crystals of boron nitride," Science **343**(6175), 1125–1129 (2014).
39. A. Kumar, T. Low, K. H. Fung, P. Avouris, and N. X. Fang, "Tunable light–matter interaction and the role of hyperbolicity in graphene–hBN system," Nano Lett. **15**(5), 3172–3180 (2015).
40. S. Dai, Q. Ma, M. K. Liu, T. Andersen, Z. Fei, M. D. Goldflam, M. Wagner, K. Watanabe, T. Taniguchi, M. Thiemens, F. Keilmann, G. C. A. M. Janssen, S.-E. Zhu, P. Jarillo-Herrero, M. M. Fogler, and D. N. Basov, "Graphene on hexagonal boron nitride as a tunable hyperbolic metamaterial," Nat. Nanotechnol. **10**(8), 682–686

Optics EXPRESS

(2015).
41. A. Woessner, M. B. Lundeberg, Y. Gao, A. Principi, P. Alonso-González, M. Carrega, K. Watanabe, T. Taniguchi, G. Vignale, M. Polini, J. Hone, R. Hillenbrand, and F. H. Koppens, "Highly confined low-loss plasmons in graphene-boron nitride heterostructures," Nat. Mater. **14**(4), 421–425 (2015).
42. H. Hajian, A. Ghobadi, S. Abedini Dereshgi, B. Butun, and E. Ozbay, "Hybrid plasmon–phonon polariton bands in graphene–hexagonal boron nitride metamaterials," J. Opt. Soc. Am. B **34**(7), D29–D35 (2017).
43. B. Zhao and Z. M. Zhang, "Resonance perfect absorption by exciting hyperbolic phonon polaritons in 1D hBN gratings," Opt. Express **25**(7), 7791–7796 (2017).
44. B. Zhao and Z. M. Zhang, "Perfect mid-infrared absorption by hybrid phonon-plasmon polaritons in hBN/metal grating anisotropic structures," Int. J. Heat Mass Transfer **106**, 1025–1034 (2017).
45. H. Hajian, A. Ghobadi, B. Butun, and E. Ozbay, "Nearly perfect resonant absorption and coherent thermal emission by hBN-based photonic crystals," Opt. Express **25**(25), 31970–31987 (2017).
46. J. Wu, H. Wang, L. Jiang, J. Guo, X. Dai, Y. Xiang, and S. Wen, "Critical coupling using the hexagonal boron nitride crystals in the mid-infrared range," J. Appl. Phys. **119**(20), 203107 (2016).
47. J. Wu, L. Jiang, J. Guo, X. Dai, Y. Xiang, and S. Wen, "Turnable perfect absorption at infrared frequencies by a Graphene-hBN Hyper Crystal," Opt. Express **24**(15), 17103–17114 (2016).
48. V. W. Brar, M. S. Jang, M. Sherrott, J. J. Lopez, and H. A. Atwater, "Highly confined tunable mid-infrared plasmonics in graphene nanoresonators," Nano Lett. **13**(6), 2541–2547 (2013).
49. Y. Liu and R. F. Willis, "Plasmon-phonon strongly coupled mode in epitaxial graphene," Phys. Rev. B **81**(8), 081406 (2010).
50. R. J. Koch, Th. Seyller, and J. A. Schaefer, "Strong phonon-plasmon coupled modes in the graphene/silicon carbide heterosystem," Phys. Rev. B **82**(20), 201413 (2010).
51. V. W. Brar, M. S. Jang, M. Sherrott, S. Kim, J. J. Lopez, L. B. Kim, M. Choi, and H. Atwater, "Hybrid surface-phonon-plasmon polariton modes in graphene/monolayer h-BN heterostructures," Nano Lett. **14**(7), 3876–3880 (2014).
52. Y. Jia, H. Zhao, Q. Guo, X. Wang, H. Wang, and F. Xia, "Tunable plasmon–phonon polaritons in layered graphene–hexagonal boron nitride heterostructures," ACS Photonics **2**(7), 907–912 (2015).
53. G. W. Hanson, "Quasi-transverse electromagnetic modes supported by a graphene parallel-plate waveguide," J. Appl. Phys. **104**(8), 084314 (2008).
54. H. Hajian, A. Soltani-Vala, and M. Kalafi, "Optimizing terahertz surface plasmons of a monolayer graphene and a graphene parallel plate waveguide using one-dimensional photonic crystal," J. Appl. Phys. **114**(3), 033102 (2013).
55. L. A. Falkovsky, "Optical properties of graphene," J. Phys. Conf. Ser. **129**, 012004 (2008).
56. Lumerical Solutions, Inc., *http://www.lumerical.com/tcadproducts/fdtd*.
57. R. Alaee, M. Albooyeh, and C. Rockstuhl, "Theory of metasurface based perfect absorbers," J. Phys. D Appl. Phys. **50**(50), 503002 (2017).
58. Z. Jacob and E. E. Narimanov, "Optical hyperspace for plasmons: Dyakonov states in metamaterials," Appl. Phys. Lett. **93**(22), 221109 (2008).
59. P. Li, I. Dolado, F. J. Alfaro-Mozaz, A. Yu. Nikitin, F. Casanova, L. E. Hueso, S. Vélez, and R. Hillenbrand, "Optical nanoimaging of hyperbolic surface polaritons at the edges of van der Waals materials," Nano Lett. **17**(1), 228–235 (2017).
60. F. J. Alfaro-Mozaz, P. Alonso-González, S. Vélez, I. Dolado, M. Autore, S. Mastel, F. Casanova, L. E. Hueso, P. Li, A. Y. Nikitin, and R. Hillenbrand, "Nanoimaging of resonating hyperbolic polaritons in linear boron nitride antennas," Nat. Commun. **8**, 15624 (2017).
61. P. Li, I. Dolado, F. J. Alfaro-Mozaz, F. Casanova, L. E. Hueso, S. Liu, J. H. Edgar, A. Y. Nikitin, S. Vélez, and R. Hillenbrand, "Infrared hyperbolic metasurface based on nanostructured van der waals materials," Science **359**(6378), 892–896 (2018).
62. L. Novotny and B. Hecht, Principles of Nano-Optics (Cambridge University Press, 2012).
63. P. Li, I. Dolado, F. J. Alfaro-Mozaz, F. Casanova, L. E. Hueso, S. Liu, J. H. Edgar, A. Y. Nikitin, S. Vélez, and R. Hillenbrand, "infrared hyperbolic metasurface based on nanostructured van der waals materials," Appl. Phys. Lett. **99**, 211106 (2011).

1. Introduction

Metamaterials, which are artificial structures with unit cells of the sub-wavelength scale, have attracted extensive research interest due to their various exotic characteristics that are unavailable in nature [1]. Nearly perfect absorption is one of the distinguished features of these structures that play a key role in many applications, such as photodetectors [2], photovoltaics [3], sensing [4-5], spectroscopy [6], etc. In order to realize nearly perfect absorption, reflectance is suppressed by matching the effective impedance of the metamaterial to that of the incident medium [7]. Simultaneously, transmittance is eliminated by introducing another metallic plate acting as a mirror [8]. Based on this mechanism, plasmonic absorbers operating in the visible, infrared (IR) and terahertz ranges with resonators of different

Optics EXPRESS

geometrical patterning, including e. g., disks [9], strips [10], crosses [11], arrows [12], and L-shaped structures [13], have been designed and investigated comprehensively. Moreover, by combining multiple resonators with different sizes together to form a super unit cell and using lithography free metal-insulator multilayer stacks, multi-channel [14, 15] and broadband [16–19] nearly perfect absorbers have also been achieved. As a plasmonic material, graphene is also capable of supporting low-loss, highly confined and tunable (by chemical doping or electrostatic/magnetostatic gating) surface plasmon polaritons (SPPs) from terahertz (THz) to the mid-infrared (mid-IR) range [20–22]. Therefore, a great diversity of plasmonic metamaterials based on this material has also been devised for enhancing light absorption, such as graphene discs [23], ellipses [24], hole arrays [25, 26], ribbons [27–31], rings [32], and graphene-based photonic crystals and hyperbolic metamaterials [33–35]. Alongside noble metals and graphene, polar dielectrics also offer an opportunity for simultaneous sub-diffractional confinement through the stimulation of surface phonon polariton (SPhP) modes [36]. SPhPs originate from the interaction of optical phonons with long-wavelength incident fields, creating a surface excitation mediated by the atomic vibrations. Such SPhP modes can be stimulated between the longitudinal optical (LO) and transverse optical (TO) phonon frequencies of the polar dielectrics. This spectral range is referred to as the Reststrahlen (RS) band or polaritonic gap. Due to the support of SPhPs, polar-based metamaterials have been considered as distinguished candidates for light absorption and coherent thermal emission in the mid- and far-IR ranges [36].

Hexagonal boron nitride (hBN) is another type of polar materials operating in the mid-IR range. As a natural hyperbolic material, the dielectric constants of hBN are the same in the basal plane ($\varepsilon_t \equiv \varepsilon_x = \varepsilon_y$) but have opposite signs ($\varepsilon_x \varepsilon_z < 0$) in the normal direction (ε_z) in the mid-IR region [37–44]. Owing to this property, finite-thickness slabs of hBN are capable of supporting sub-diffractional volume-confined polaritons and can act as multimode waveguides for the propagation of hyperbolic phonon polariton collective modes for TM polarization [39]. Following [40, 42], we label the graphene SPPs and hyperbolic phonon polaritons of a thin film of hBN as SP^2 and HP^2 modes, respectively. It has been recently reported that, due to the support of HP^2 modes, 1D grating of hBN is capable of supporting highly concentrated resonant absorption for TM polarization [43]. As a result of the coupling of magnetic polaritons in metal gratings with HP^2 of hBN, nearly perfect absorption for TM polarization can also be observed by an unpatterned film of hBN on top of a metallic grating [44]. Due to the support of Tamm phonons, it is also possible to obtain nearly perfect resonant absorption, for both TM and TE polarizations, using unpatterned films of hBN in one-dimensional photonic crystals [45-46]. Moreover, graphene-hBN hypercrystal is capable of mid-IR nearly perfect light absorption as well, provided that extremely large number of graphene-hBN unit cells being used [47].

According to the above-mentioned eye-catching characteristics of graphene SPPs and the phonon polaritons of polar materials in the THz and IR regions, heterostructures combining graphene and polar dielectrics might yield unique and useful optical responses. Recent experimental and theoretical studies on graphene on SiO_2 [29, 48] and SiC [49, 50] substrates have shown that the graphene dispersion relation in the mid-IR range can be significantly modified due to the substrate phonons with extra modes arising due to plasmon-phonon coupling. This coupling has been considered as surface plasmon-phonon polaritons [51]. In [51, 52], by fabricating patterned graphene/monolayer-hBN and graphene/triple-layer-hBN structures, it was proven that graphene plasmons can couple to optical excitations that occupy an atomically thin slice of volume near the graphene. In this case, a small modal volume of the graphene plasmons can be combined with the high oscillator strength of the hBN phonons that allows the two modes to strongly couple. Moreover, by combining graphene with hBN films (>10 nm) in multilayer structures, one can also efficiently tune the hyperbolic dispersion of hBN phonons using graphene plasmons, i.e. the appearance of hybrid plasmon-phonon polaritons (HPPs) [39–42]. HPPs can be categorized to hyperbolic plasmon-phonon

Optics EXPRESS

polaritons (HP^3) and surface plasmon-phonon polaritons (SP^3) that are supported inside and outside of the RS bands of hBN, respectively [40, 42]. However, to our knowledge, the resonant plasmonic-phononic effects in the patterned graphene-hBN metamaterials that are observed due to the support of SP^3 and HP^3 modes has not been investigated to the present.

In the present paper, by taking advantage of plasmon-phonon hybridization in a graphene-hBN-based metamaterial, we obtain nearly perfect multi-resonant absorptions with omnidirectional and tunable characteristics, for both polarizations in the mid-IR range. The metamaterial is composed of a 300 nm film of hBN bounded by two graphene layers on top of a 200 nm-thick film of gold, separated by a transparent dielectric layer. The multilayer graphene/hBN/graphene is considered to be patterned as a hole array in a square lattice. It is shown that due to the hybridization of graphene SP^2s and hBN HP^2s and thereby the appearance of SP^3 and HP^3 resonances, the metamaterial can support nearly perfect resonant absorptions both inside and outside of the RS band of hBN that makes this design beneficial for multifunctional operations. Since the anti-dot, hole array, patterning of the structure keeps the graphene layers continuous, the obtained resonances can be effectively tuned by gating. Moreover, we show that, in contrast with the graphene-based metamaterials [25, 26], the strengths and full width at half maximum (FWHM) of the absorption peaks in the graphene-hBN-based metamaterial are weakly affected by the phenomenological relaxation time of electrons in graphene. To our knowledge, this is the first demonstration of nearly perfect resonant light absorptions in graphene/hBN heterostructures, with the aforementioned skeptical features, that can be of great interest for sensing applications in the id-IR range.

2. Resonant absorptions in a graphene-based hole array metamaterial

In order to get more insight into the absorption mechanisms and absorption resonances of the final design, first, we would like to investigate, respectively, graphene-based and hBN-based hole array metamaterials in this section and in the next one, separately. The schematic of the graphene-based metamaterial is illustrated in panel (a) of Fig. 1. As shown in Fig. 1(a), the graphene-based hole array metamaterial is composed of graphene/dielectric/graphene multilayer on top of a gold layer (t_m), separated by a dielectric spacer layer of width t_s and ε_s. The thickness and refractive index of the dielectric layer in between the two graphene layers are t_h and ε_s, respectively. Moreover, the graphene/dielectric/graphene multilayer is periodically patterned in a square lattice with holes of radius R and periodicity L. In order to analyze the resonant absorption peaks of the graphene-based metamaterial, SP^2 dispersion curves of a double-layer graphene waveguide should be examined. Taking the y component of the magnetic field as

$$H_y(z)=\begin{cases} ae^{-q_a(z-t_h/2)}, & z>t_h/2 \\ h_1e^{-q_sz}+h_2e^{q_sz}, & -t_h/2\le z\le t_h/2, \\ se^{q_s(z+t_h/2)}, & z<-t_h/2 \end{cases} \tag{1}$$

and applying the boundary conditions for TM polarization [22], we arrive at the following dispersion relation of the SP^2 modes of the graphene/dielectric (ε_s)/graphene structure that is bounded with materials of ε_a and ε_s [53-54]:

$$\tan\mathrm{h}(q_st)=-\frac{\Gamma_a+\Gamma_s}{1+\Gamma_a\Gamma_s}. \tag{2}$$

Optics EXPRESS

Here, $\Gamma_j = \frac{q_s}{\varepsilon_s}\left(\frac{\varepsilon_j}{q_j} - \alpha\right)$, $q_j = \sqrt{\beta^2 - \varepsilon_j \beta_0^2}\ (i = a, s)$, $\beta = k_x$, $\beta_0 = \omega / c$, and $\alpha = \frac{\sigma_g}{i\omega\epsilon_0}$. The optical conductivity of graphene ($\sigma_g = \sigma_g^{intra} + \sigma_g^{inter}$) can be presented as [55]

$$\sigma_g^{intra}(\omega) = \frac{e^2}{4\hbar}\frac{i}{2\pi}\{\frac{16k_B T}{\hbar\Omega}\ln(2\cosh(\frac{\mu}{2k_B T}))\}, \tag{3a}$$

$$\sigma_g^{inter}(\omega) = \frac{e^2}{4\hbar}\{\frac{1}{2} + \frac{1}{\pi}\arctan\left(\frac{\hbar\Omega - 2\mu}{2k_B T}\right) - \frac{i}{2\pi}\ln\frac{(\hbar\Omega + 2\mu)^2}{(\hbar\Omega - 2\mu)^2 + (2k_B T)^2}\}, \tag{3b}$$

with $\Omega = \omega + i\tau^{-1}$, e is the electron charge, k_B is the Boltzmann constant, τ is electron relation time, and $\hbar$ is the Plank constant over 2π. In the present paper, it is noteworthy that we take $T = 300K$, $\mu = 0.5eV$, $\tau = 2ps$, $\varepsilon_s = 2.25$ (e.g. BaF_2), $t_h = 300nm$, $t_s = 1\mu m$, $t_m = 200nm$, $L = 3R$, $R = 40nm$ and $\theta = 0$, *otherwise stated*. SP^2 dispersion curves are illustrated in Fig. 1(b) in the wavelength range of our interest in the mid-IR region, i.e. $5\mu m \le \lambda \le 9\mu m$. As expected [53-54], due to the coupling between the graphene layers, two SP^2 branches are shown in Fig. 1(b) that can be modified by the separation distance of the graphene sheets. In agreement with the analytically obtained SP^2 dispersions, taking $t_s = 1\mu m$, absorption of the graphene-based hole array metamaterial, that is numerically calculated using the finite difference time domain method (FDTD) [56], is also represented in Fig. 1(c) for normal incidence of light. Here we calculate absorption as $A = 1-R$. It is also noteworthy that since $t_m = 200nm$ is considerably larger than the gold skin depth ($\delta = \lambda / [2\pi Im(n_{Au})]$) in the mid-IR range ($0.153 < \delta / t_m < 0.183$), it guarantees that the bottom layer acts as a perfect mirror. Moreover, it should be noted that for all mode profiles represented in this paper the monitors are placed on top and center of the unit cell for top- and side-views, respectively.

Optics EXPRESS

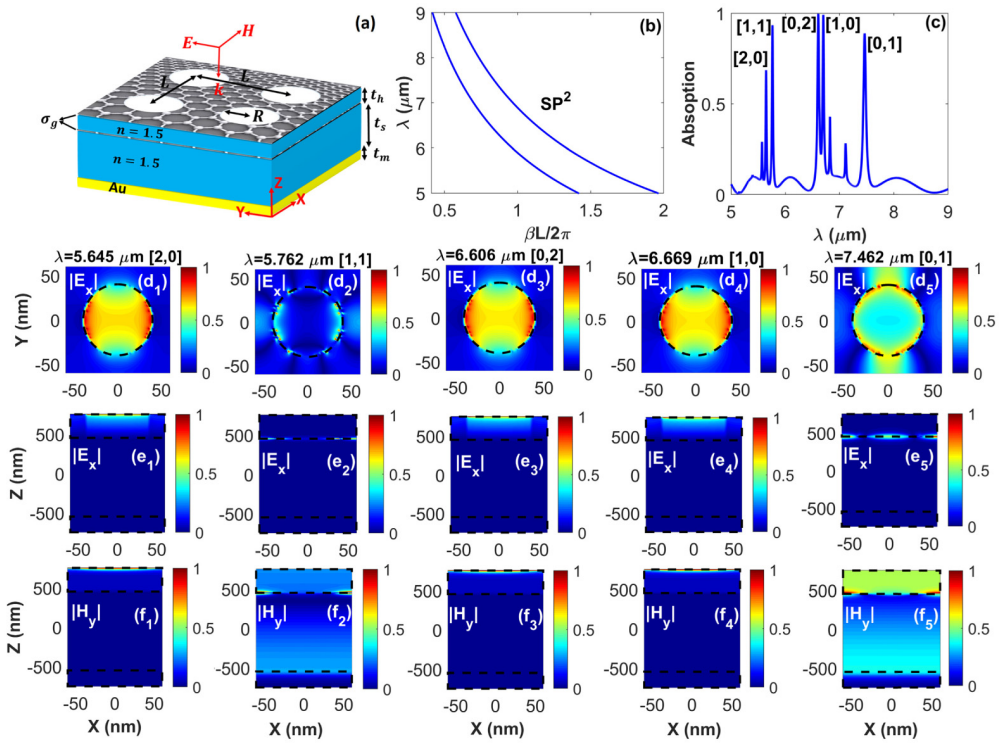

Fig. 1. (a) Schematic of the graphene-based hole-array metamaterial, (b) dispersion curves of SPPs supported by a graphene/dielectric/graphene waveguide, and (c) absorption plot of the metamaterial shown in panel (a). Panels (d_j), (e_j) and (f_j) [j = 1,…,5], respectively, illustrate normalized $|E_x|$ top view, $|E_x|$ side view and $|H_y|$ side view mode profiles at different absorption peaks shown in panel (c). The dashed circles in panels (d_j) highlight the hole position in each unit cell, and the dashed rectangles in panels (e_j) and (f_j) distinguish the position of the top dielectric layer and the bottom gold layer. In our calculation, $R = 40\ nm$, $L = 3R$, $t_h = 300\ nm$, $t_s = 1\ \mu m$ and $t_m = 200\ nm$.

It is seen in Fig. 1(c) that strong resonant absorptions at five wavelengths are observed by the graphene-based hole array metamaterial. This large number of the plasmonic resonances are in fact due to the coupling between SP^2s supported by the upper and downer graphene sheets, and consequently can be increased by decreasing t_h. More investigations prove that, in case of removing the downer (upper) graphene layer, the number of resonances will be decreased to two (three), confirming the noticeable effect of support of the coupled SP^2 modes on the number of resonant absorption peaks of the graphene-based metamaterial. Moreover, wavelengths of the plasmonic resonances can be approximately described by SP^2 excitations in different diffraction orders as

$$\lambda_P(n,m) = \frac{\beta L}{\beta_0\sqrt{n^2+m^2}}. \tag{4}$$

This is how we labeled the above-mentioned nearly perfect resonant absorption peaks as [n, m] in Fig. 1(c) [25]. However, this labeling can also be performed by the investigation of plasmonic/phononic band structure of the metamaterial, as explained in Ref. 26. Note that Eq. (4) can be employed to label the resonant plasmonic/phononic/hybrid absorption peaks due to the excitation of SP^2, HP^2, and HPPs (i.e. SP^3 and HP^3 modes). To reveal the physical mechanism leading to the observed resonant absorptions, the electric and magnetic field

Optics EXPRESS

profiles ($|E_x|$ and $|H_y|$) at those five peaks are also illustrated in Figs. 1(d_j) [top view of $|E_x|$], 1(e_j) [side view of $|E_x|$], and 1(f_j) [top view of $|H_y|$] where j = 1,…,5. As seen from the top view mode profiles, the five peaks illustrate the plasmonic resonances excited at the edges of the graphene holes. More specifically, through the investigation of Re(E_x) of these mode profiles we understood that [2,0], [0,2], [1,0] modes resemble the ones supported by similar metallic structures [9] and [1,1] and [0,1] modes are similar to the whispering-gallery resonances in the single-layer graphene-based hole array metamaterial [25]. Side view $|E_x|$ profiles uncovers that for [2,0], [0,2], and [1,0] resonances the upper graphene layer is mostly responsible for the light absorption, while for the [1,1] and [0,1] resonances the downer one is more activated. Moreover, it is observed from $|H_y|$ mode profiles that there is not any near-field interaction between the graphene layers and the bottom gold layer for [2,0], [0,2], and [1,0] modes, thus no propagating or localized SP^2 modes is supported. Similar mechanism, named as Salisbury absorption, has been also reported for light absorption by single layer graphene ribbons [27, 57]. On the other hand, $|H_y|$ profiles of [1,1] and [0,1] modes show that the magnetic field is resonantly enhanced around the interface separating the dielectric gap spacer and the bottom reflector layer, proving the lateral interaction between the adjacent graphene holes. This is the indication of supporting propagating SP^2s by the structure. The same mechanism is observed in a metamaterial absorber composed of double layer graphene ribbons [30, 31]. It is noteworthy that for the light absorption obtained by metal/insulator/metal hole array and disc array metamaterial both localized and propagating SPPs are responsible [9]. For the propagating SPPs the magnetic field is not only confined in the gap region underneath the holes/discs, but also strongly enhanced between them. While for the localized SPPs the magnetic field is mainly concentrated within the gap between the topmost holes/dots and the gold underlay.

3. Resonant absorptions in a hBN-based hole array metamaterial

The next structure that we analyze in this paper is a hole array metamaterial absorber based on hBN. The schematic of this structure is shown in Fig. 2(a). Similar to the design shown in Fig. 1(a), the top layer (hBN film) is patterned as hole arrays in square lattice with periodicity L and is placed on top of the gold bottom layer, separated by a dielectric spacer. In order to be able to approximately label the resonances supported by the hBN-based metamaterial we need to inspect the dispersion of hyperbolic phonon polaritons, HP^2 modes, of a film of hBN that is bonded with air and a material with ε_s. In our calculations, the hBN layer is modeled as a uniaxially anisotropic medium of thickness t_h and a permittivity tensor $\varepsilon_{hBN} = diag(\varepsilon_t, \varepsilon_t, \varepsilon_z)$ for which

$$\varepsilon_m = \varepsilon_{\infty,m} \times \left[1 + \frac{\omega_{LO,m}^2 - \omega_{TO,m}^2}{\omega_{TO,m}^2 - \omega^2 - i\omega\Gamma_m} \right], m = t, z, \tag{5}$$

where $\varepsilon_{\infty,x} = 2.95$, $\varepsilon_{\infty,z} = 4.87$, $\omega_{LO,x} = 1610\,cm^{-1} (\equiv 6.2\mu m)$, $\omega_{TO,x} = 1370\,cm^{-1} (\equiv 7.3\mu m)$, $\omega_{LO,z} = 830cm^{-1}$, $\omega_{TO,z} = 780cm^{-1}$, $\Gamma_x = 4cm^{-1}$ and $\Gamma_z = 5cm^{-1}$ [34]. $Re(\varepsilon_x)$ [solid blue], $Im(\varepsilon_x)$ [dotted-blue], $Re(\varepsilon_z)$ [solid black], $Im(\varepsilon_z)$ [dotted black] are illustrated in the inset of Fig. 2(c) in the wavelength of our interest ($5\mu m \le \lambda \le 9\mu m$). Notice that the vertical dashed lines in this figure represent the boundaries of the RS-II band of hBN ($\varepsilon_x < 0$ and $\varepsilon_z > 0$) at $6.2\mu m$ and $7.3\mu m$. Taking H_y similar to that of Eq. (1) and applying the appropriate boundary condition for TM polarization [42], the following dispersion relation for the hyperbolic phonon polaritons of hBN, HP^2s, is obtained

Optics EXPRESS

$$\tan\mathrm{h}\left(q_h t\right) = -\frac{\Gamma_a + \Gamma_h}{1 + \Gamma_a \Gamma_h} \tag{6}$$

where $\Gamma_j = \frac{q_h}{\varepsilon_x}\left(\frac{\varepsilon_j}{q_j}\right)(\mathrm{j=a,s})$ and $q_h = \sqrt{\varepsilon_x(\beta^2 - \varepsilon_z \beta_0^2)/\varepsilon_z}$.

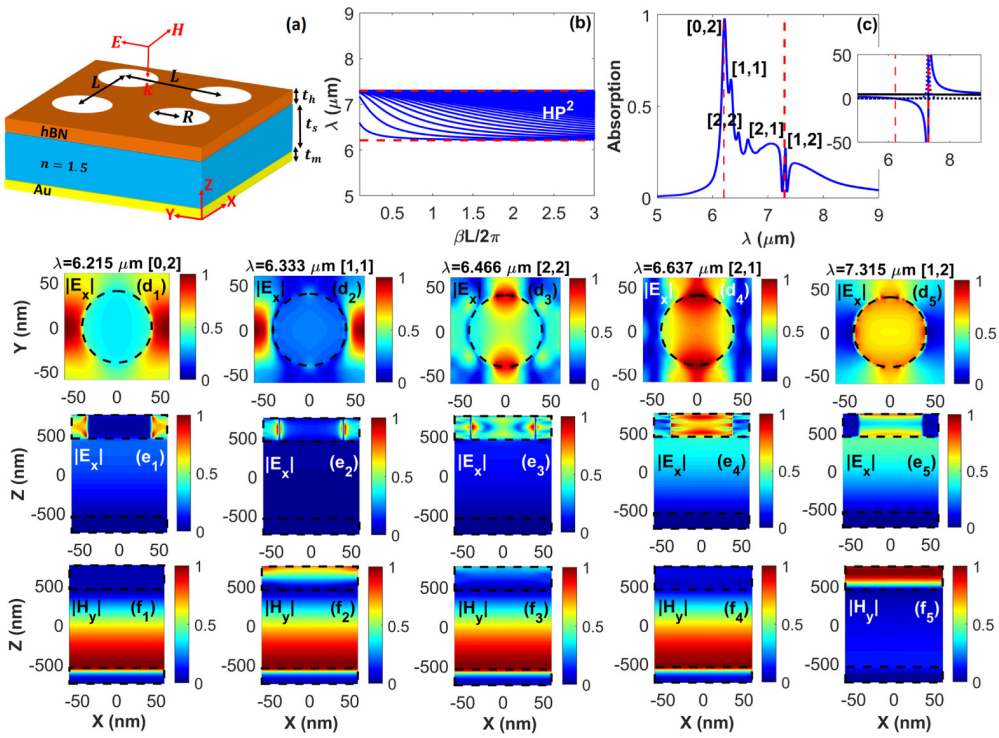

Fig. 2. (a) Schematic of the hBN-based metamaterial. The hBN layer is patterned as a hole array in square lattice with periodicity *L*. (b) Dispersion curves of the hyperbolic phonon polaritons, HP^2s, supported by a film of hBN. Absorption plot of the structure is illustrated in panel (c) and, $Re(\varepsilon_x)$ [solid blue], $Im(\varepsilon_x)$ [dotted-blue], $Re(\varepsilon_z)$ [solid black], $Im(\varepsilon_z)$ [dotted black] are shown in the inset. Horizontal [vertical] dashed lines in panel (b) [(c)] highlight the edges of the RS-II band of hBN. Top view [side view] of normalized $|E_x|$ and side view of normalized $|H_y|$ are represented in panels (d_j) [(e_j)] and (f_j), respectively (j = 1,…,5). The hole position in each unit cell and the position of hBN and gold bottom layers are highlighted with dashed circles and rectangles. In the calculations, we took R = 40 nm, L = 3R, t_h = 300 nm, t_s = 1 μm and t_m = 200 nm.

Figure 2(b) provides a dispersion of the hyperbolic phonon-polaritons of 300 nm film of hBN that is bounded by air and a material with ε_s. In agreement with the results in the literature [39], this slab of hBN supports several closely separated branches of phonon-polaritons. Since the phonon-polaritons are supported in the RS-II band, they possess the second type of hyperbolicity. The resonant absorption peaks of the metamaterial are illustrated in Fig. 2(c) and labeled as [n,m] resonances. Notice that we performed this labeling by approximately matching the condition of HP^2 excitation in different diffraction orders by using the data obtained from the dispersion curves [Fig. 2(b)] in Eq. (4). Once the electric field of the incident light is parallel to the direction along which the permittivity is the most negative, both strong and weak series of resonant absorption peaks are supported by the hBN-based metamaterial. In agreement with [34], Fig. 2(c) shows the strength of the resonances

Optics EXPRESS

reduced inside the RS-II band by increasing the wavelength. Further insight into the nature of the resonant modes is obtained by examining their electric and magnetic field mode profiles; see Figs. 2(d_j) [top view of $|E_x|$], 2(e_j) [side view of $|E_x|$], and 2(f_j) [top view of $|H_y|$] where j = 1,…,5. Top view mode profiles reveals how the resonances are excited inside the hBN layer. In addition, side view electric field mode profiles [Fig. 2(e_j)] clearly prove the support of hyperbolic phonon-polariton rays, HP^2 rays, at the resonant wavelengths. To be specific, it is observed that HP^2 rays are supported through three different mechanisms: (i) inside the hBN film for [0,2] mode [Fig. 2(e_1)], (ii) inside the hole for [1,2] resonance [Fig. 2(e_5)], and (iii) mixture of the first and the second mechanism that is observed from side view of $|E_x|$ mode profiles of [1,1], [2,2], and [2,1] modes shown in Fig. 2($e_{j=2,3,4}$). Consequently, in contrast to the hBN nanoparticles where the modes are confined inside the patches [34], here the rays zigzag and experience total internal reflection inside the hole array hBN metamaterial in three aforementioned different ways. It is noteworthy that the cross-hatch patterned observed in Fig. 2($e_{j=1,\ldots,5}$) is the sign of directionality of HP^2 propagation for which the angle between the high-field crossing lines and the z axis is numerically close to $\Theta(\omega)=\frac{\pi}{2}-\arctan(\sqrt{\varepsilon_z(\omega)}/i\sqrt{\varepsilon_t(\omega)})$ [34]. Moreover, the considerable enhancement of the magnetic field inside the spacer layer [see 2($f_{j=1,2,3,4}$)] indicate the near-field interaction of the top hBN layer with the bottom gold reflector, proving this point that the propagating HP^2 modes are responsible for the resonant absorptions observed for [0,2], [1,1], [2,2], and [2,1] modes.

In addition to the support of HP2 modes, it has been recently discovered that hBN-based metamaterials composed of rectangular components are also capable of supporting hyperbolic surface phonon polaritons (HSPs). These modes are a special type of Dyakonov surface waves [58] which emerge when the optical axis of hBN lies in the interface plane separating hBN and the isotropic medium [59–61]. In these papers it is explained that HSPs can be supported by thin hBN flakes once the structure is excited in an appropriate direction with respect to its optical axis. More specifically, in case the structure is properly excited from the edge, hyperbolic bulk phonon polaritons can spread inside the thin hBN flakes and HSPs can propagate along the edges (sidewalls) of the structure, which form a natural two-dimensional waveguide for HSPs. It is noteworthy that to understand the possibility of exciting HSPs in the structures under our consideration in this paper, we further investigated mode profiles of resonant absorptions of a hBN-based metamaterial composed of rectangular holes. We understood that by appropriately designing the system, it is possible to uncover the role of HSPs in the absorption peaks by looking at the mode profiles at the edge of the holes.

4. Resonant absorptions in a graphene-hBN-based hole array metamaterials

The last design we investigate is a combination of the structures shown in Figs. 1(a) and 2(a). As represented in Fig. 3(a), this metamaterial is composed of a patterned graphene/hBN/graphene multilayer on a gold bottom layer separated by a dielectric spacer. Similar to the previous structures, the graphene/hBN/graphene multilayer is patterned as a hole array in a square lattice with a periodicity of L. Analogous to the recent cases, here, to be able to label the resonant modes, we first examine the dispersion curves of the hybrid plasmon-phonon polaritons, HPPs. These modes are supported by the graphene/hBN/graphene waveguide that is bounded by air and the material with a dielectric constant of ε_s. The dispersion relation of the HPPs can be obtained by replacing

$$\Gamma_j=\frac{q_h}{\varepsilon_x}\left(\frac{\varepsilon_j}{q_j}-\alpha\right)(\mathrm{j}=\mathrm{a},\mathrm{s}) \tag{7}$$

Optics EXPRESS

with its older version in Eq. (6). The corresponding dispersion curves are represented in Fig. 3(b).

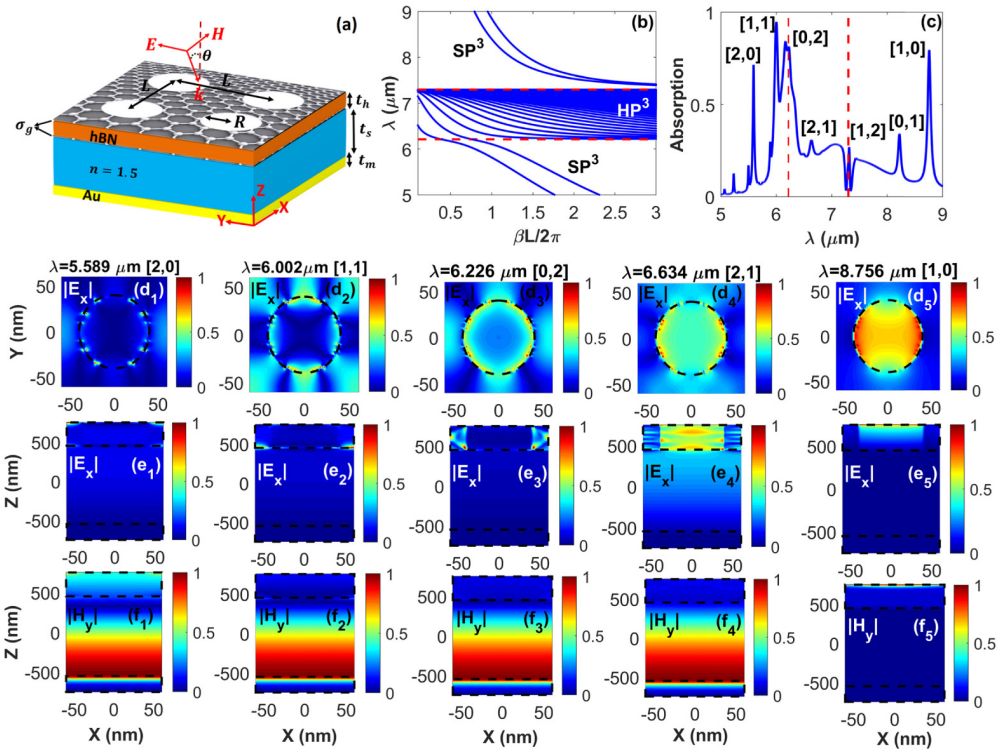

Fig. 3. Schematic of the graphene-hBN-based metamaterial is shown in panel (a) for which the graphene/hBN/graphene multilayer is patterned as a hole array in square lattice with periodicity L. The dispersion curves of the hybrid plasmon-phonon polaritons (SP^3s and HP^3s) of the graphene/hBN/graphene waveguide are represented in panel (b). The absorption plot of the metamaterial is represented in panel (c). The edges of the RS-II band of hBN are also highlighted with horizontal [vertical] dashed lines in panel (b) [(c)]. The arrangements of profiles of the normalized electric and magnetic fields and also the taken geometrical parameters are the same as Figs. (1) and (2).

It is clearly observed from Fig. 3(b) that, due to the plasmon-phonon hybridization, the graphene/hBN/graphene heterostructure supports HPPs that have hyperbolic phonon polariton (HP^2) dispersion characteristics inside the RS-II band of hBN. These modes are thus labeled as HP^3 ones. On the other hand, the modes supported outside of the RS-II band are labeled as SP^3 modes since they mostly possess the characteristics of SP^2 surface plasmons. In other words, dispersion curves of the SP^3 and HP^3 modes in Fig. 3(b) resemble those of SP^2s and HP^2s in Figs. 1(b) and 2(b), respectively (this point will be more clarified by analyzing the mode profiles). The resonant absorption peaks of the graphene-hBN-based hole array metamaterial are also represented in Fig. 3(c) and labeled by combining the data of Fig. 3(b) with Eq. (4). As seen, for [2,0], [1,1], [0,2], and [0,1] modes the metamaterial acts as nearly-perfect absorber. It is noteworthy that one of the interesting outcomes of the plasmon-phonon hybridization in the graphene/hBN/graphene heterostructure is the smooth merging of the two lowest branches of the HP^2 modes in Fig. 2(b) into the HP^3-SP^3 modes around the edge of the RS-II band at $\lambda = 6.2\mu m$ in Fig. 3(b). This merging characteristic is, in fact, due to the transition of hBN response from hyperbolic to elliptical. As illustrated in Fig. 3(c), this merging feature leads to the appearance of two closely separated nearly perfect absorption

Optics EXPRESS

peaks around $\lambda = 6.2\mu m$, but with different characteristics [see the mode profiles in Fig. 3]. Moreover, since presence of the graphene layers has a considerable impact on the coupling efficiency of the plasmonic and phononic modes, number of the resonances can be decreased to three (four) by removing the upper (downer) graphene layer. The mode profiles of the five most important resonances in Fig. 3(c) are also illustrated in Figs. 3(d_j), 3(e_j), and 3(f_j). Top and side view $|E_x|$ profiles of [2,0] and [1,1] modes in Figs. 3($d_{1,2}$) and 3($e_{1,2}$) resemble those illustrated in Figs. 2($d_{1,2}$) and 2($e_{1,2}$), approving this point that [2,0] and [1,1] SP^3 resonance have plasmonic characteristics. The same resemblance holds for $|E_x|$ profiles of [1,0] mode depicted in Figs. 3(d_5) and 3(e_5). Similarly, Figs. 3(e_3) and 3(e_4) obviously look like those of [0,2] and [2,1] modes in Figs. 2(e_1) and 2(e_4), confirming phononic nature of the [0,2] and [2,1] HP^3 modes. Moreover, the side view profiles of $|H_y|$ show the considerable impact of the hBN phonons on the absorption mechanism of the graphene-hBN-based hole array metamaterial; i.e. there is a strong resonant interaction between the graphene/hBN/graphene multilayer and the bottom gold reflector. Therefore, the support of propagating SP^3 ([2,0] and [1,1] modes) and propagating HP^3 modes ([0,2] and [2,1] modes) are responsible for the light absorption, while the cause for [1,0] mode absorption is the Salisbury mechanism. It is noteworthy that we also analyzed the results for $t_h = 400\ nm$ and $200\ nm$. It was understood that considering $t = 400\ nm$ in the calculations leads to support of stronger absorption peaks inside the RS-II band in Figs. 2(b) and 3(b). However, that choice makes the plasmonic resonances weaker outside of the RS-II band in Fig. 3(b). The situation is reversed for the case of $t_h = 200\ nm$. Therefore, we considered $t_h = 300\ nm$ to keep both SP^3 and HP^3 resonances strong enough. This is the maximum thickness that a graphene layer can well affect the response of hBN [40].

As mentioned hereinabove, the optical impedance matching plays an important role in obtaining nearly-perfect absorption [7]. To get further insight into the absorption mechanism of our structure, shown in Fig. 3(a), we retrieve the corresponding effective optical impedance ($Z_{eff} = Z'_{eff} + iZ''_{eff}$) and the reflection coefficient (Γ) of the structure using

$$Z_{eff} = \sqrt{\frac{(1+S_{11})^2 - S_{21}^2}{(1-S_{11})^2 - S_{21}^2}} \tag{8a}$$

and

$$\Gamma = \left|\frac{Z_{eff} - 1}{Z_{eff} + 1}\right|. \tag{8b}$$

Here, S_{11} and S_{21} are scattering matrix coefficients that, respectively, correspond to the reflection and transmission of normally incident light. As expected, our calculations show that S_{21} is almost zero due to the presence of the thick gold bottom layer.

Optics EXPRESS

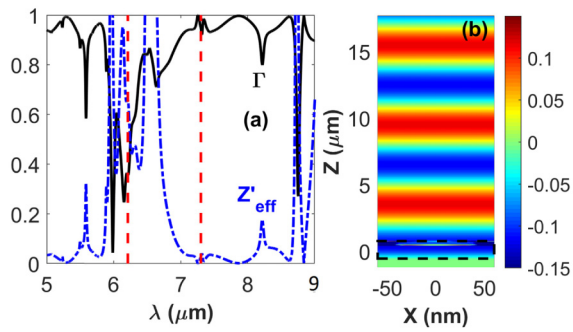

Fig. 4. (a) Reflection coefficient (Γ) and effective impedance (Z'_{eff}) of the graphene-hBN-based hole array metamaterial at normal incidence. Plot of Ex in panel (b) visualizes the impedance-matching condition between incident light and the metamaterial at a typical resonant wavelength (i.e. 6.002 μm). The metamaterial in this panel is highlighted by a dashed rectangle.

In support of Fig. 3(c), solid-black and dashed-blue curves in panel (a) of Fig. 4 show plots of Γ and Z'_{eff} of the graphene-hBN-based metamaterial, respectively. It is clearly observed that for the nearly-perfect resonant absorptions, i.e. nearly-zero resonant reflections, the effective impedance of the metamaterial is close to one. This verifies that the impedance-matching condition is satisfied at nearly-perfect absorption resonances. As a more visualized proof of the satisfaction of the impedance-matching condition, as a typical example, the E_x profile of [1,1] mode in Fig. 3 is also provided in Fig. 4(b). It is obvious that at $\lambda = 6.002\mu m$ light penetrates inside the metamaterial without being reflected noticeably.

It should be pointed out that, in practice, light usually impinges onto the structure under oblique incidences [from a practical point of view, this incident angle is usually realized within 0 to 60° in ellipsometric measurements]. Thus, the absorption of the graphene-hBN-based metamaterial as a function of the wavelength and angle of incidence is examined in Fig. 5(a) for 0<θ<60°. Based on this color map, it is observed that the resonant absorption peaks supported by the metamaterial possess omnidirectional characteristic while keeping their strength as high as the case of normal incidence up to $50°$. It is noteworthy that since the decrease in the strength of the resonances is not considerable for 50°<θ<60°, we mentioned omnidirectionality as a characteristic of the structure. It should be highlighted that more investigations reveal that, due to the structural symmetry, the angular dependency of absorption for TE polarization is almost the same as the case of TM polarization. Moreover, as a complementary discussion, Figs. 5(b) and 5(c) are also provided to indicate this point that we chose $L = 3R$ and $t_s = 1\ \mu m$ to keep resonances both inside and outside of the RS-II region strong enough.

Optics EXPRESS

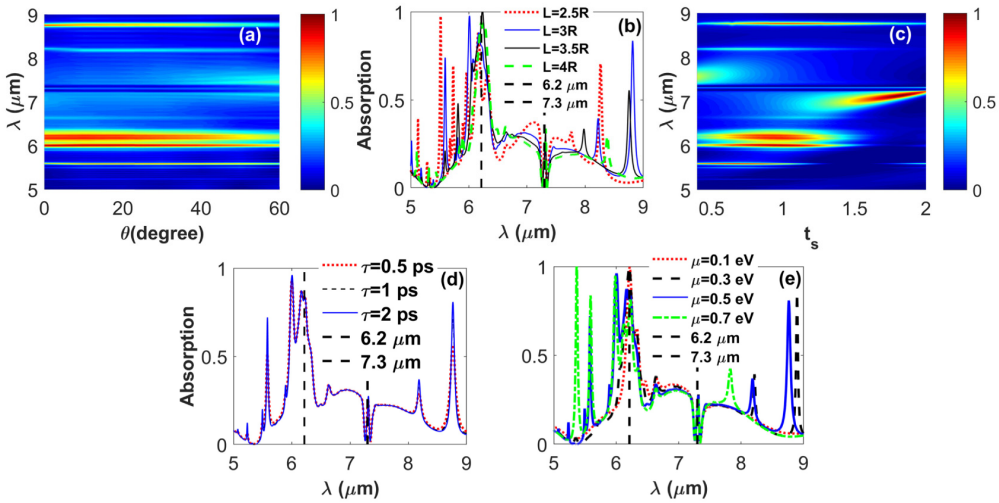

Fig. 5. (a) TM polarization absorption as a function of wavelength and angle of incidence. (b) absorption of the graphene-hBN-based metamaterial for different values the hole array periodicity. Absorption as a function of wavelength and the thickness of the dielectric spacer layer is illustrated in panel (c). Panels (d) and (e) represent absorption of the metamaterial for different values of τ and μ of the graphene layers, respectively.

As predicted numerically [25] and verified experimentally [26], the resonant plasmonic effects in graphene-based metamaterials are a strong function of the phenomenological relaxation time of electrons inside graphene (τ). In other words, as reported [25, 26], the high quality factor (Q_F) and strong resonances that are observed in the numerical calculations for large values of τ (τ~1 ps), turned out to be weak resonances with small Q_F because of the small values of τ (τ~0.5 ps) in the experimental results [26]. Figure 5(d) proves that, due to the hybridization of graphene plasmons with hyperbolic phonons of hBN, the resonances around the edge of the RS-II band at 6.2 μm are almost unaffected by the decrease in τ. In addition, the SP^3 resonances that are supported far from the edge of the RS-II band are negligibly weakened due to the reduction of τ. Moreover, Q_F, the number of the resonances, and the place of the resonances can also be noticeably tuned by changing the chemical potential of the graphene layers [see Fig. 5(e)]. Furthermore, from the width of the nearly perfect absorption peaks, we estimate Q_F of the resonance in Fig. 3(c) in the range of ~61 (for [0,2] mode) to 180 (for [2,0] mode). These quality factors are comparable to that of hBN-based structure [37, 60] and SiC nanopillars [62], and higher than the Q_{Fs} reported for metal (plasmonic) antennas in the mid-infrared spectral range [63]. It is noteworthy that, due to the continuity of the graphene sheets in the hole array patterning, the tuning of the design can also be more effectively realized in the experiment. These spectacular characteristics [obtained by Figs. 5(a), 5(d) and 5(e)], make the graphene-hBN-based metamaterial an outstanding candidate for practical applications.

5. Conclusion

In conclusion, we have proposed a multi-resonant, high-Q_F, nearly perfect plasmonic-phononic absorber that operates in the mid-IR range. The absorber is based on a graphene/hBN/graphene multilayer on top of a gold reflector that is separated by a dielectric spacer. The graphene/hBN/graphene is patterned as a hole array in square lattice. We have analytically investigated the dispersion curves of the guided modes supported by a graphene/hBN/graphene waveguide and numerically analyzed the absorption spectra of the metamaterial. Through those investigations, it has been found that the hybridization of graphene plasmons with hyperbolic phonons of hBN leads to strong absorption resonances

Optics EXPRESS

that follow different mechanisms compared to the ordinary metal-based and graphene-based plasmonic absorbers. Moreover, in contrast with the graphene-based metamaterials, due to the mentioned plasmon-phonon hybridization, the high-Q_F resonances are almost unaffected by the reduction of the phenomenological relaxation time of graphene that is unavoidable in practice. Furthermore, owing to the continuous patterning of the graphene layers, the hybrid resonances can also be effectively tuned by gating. These skeptical features make the proposed graphene-hBN-based metamaterial a distinguished candidate for multifunctional sensing purposes in the mid-IR range.

Funding

This work is supported by the projects DPT-HAMIT and TUBITAK under Project Nos. 113E331, 114E374, and 115F560.

Acknowledgments

E.O. acknowledges support from the Turkish Academy of Sciences.